Bachelorarbeit

Zur Erlangung des akademischen Grades Bachelor of Science

Thema der Arbeit

Simulating the infrastructure related degradation of ice-wedge polygonal tundra along a gravel road in Prudhoe Bay, Alaska

eingereicht von: Alexander Oehme

Gutachter/innen: Dr. Moritz Langer
Prof. Dr. Christoph Schneider

Eingereicht am Geographischen Institut der Humboldt-Universität zu Berlin am:

06. Februar 2019

Simulating the infrastructure related degradation of ice-wedge polygonal tundra along a gravel road in Prudhoe Bay, Alaska

Alexander Oehme[1,2]

[1]Humboldt University of Berlin, Geography Department, Unter den Linden 6, 10099 Berlin, Germany
[2]Alfred Wegener Institute, Helmholtz Centre for Polar and Marine Research, Telegrafenberg A45, 14473 Potsdam, Germany

Correspondence: Alexander Oehme (oehmeale@hu-berlin.de)

Contents

List of Figures

List of Tables

Abstract. Due to permafrost degradation, triggered by climate warming and human activities, infrastructure in the Arctic is at particularly high risk. Linear infrastructure such as roads or railway lines can influence the evolution of polygonal tundra and enhance degradation due to changes in the hydrological conditions. In this study, the CryoGrid 3 land surface model is used to simulate the impact of different hydrological conditions triggered by a gravel road. In addition, a sensitivity analysis is performed to better understand the influence of different snow properties on the simulations. The results show that a reduced water runoff leads to a higher soil subsidence due to melting ice wedges, whereas the timing of the degradation is strongly controlled by the snow density. A more accurate determination of soil temperatures and better knowledge of stratigraphy and snow conditions could increase the accuracy of future simulations. Furthermore, factors such as snowdrifts and road dust are not taken into account yet, but might be important to consider in future studies. This will help to better understand the complex underlying processes that affect the evolution of polygonal tundra under the influence of infrastructure and changing climate conditions.

Aufgrund der Degradation des Permafrostbodens, ausgelöst durch die Klimaerwärmung und menschliche Aktivitäten, ist die Infrastruktur in der Arktis einem besonderen Risiko ausgesetzt. Lineare Infrastrukturen wie Straßen oder Schienenwege können durch Änderungen der hydrologischen Bedingungen die Entwicklung von polygonaler Tundra beeinflussen und Degradationserscheinungen verstärken. In dieser Arbeit wird mithilfe des Landoberflächenmodells CryoGrid 3 simuliert, wie sich unterschiedliche hydrologische Bedingungen ausgelöst durch eine Kiesstraße auf den Permafrost auswirken. Zusätzlich wird durch die Veränderung der Schneedichte in den Simulationen die Sensitivität des Modells gegenüber unterschiedlichen Schneebedingungen getestet. Die Ergebnisse haben gezeigt, dass ein verringerter Wasserabfluss zu einer stärkeren Bodenabsenkung durch schmelzende Eiskeile führt, während der Zeitpunkt der Degradation maßgeblich von der Schneedichte abhängt. Eine genauere Bestimmung der anfänglichen Bodentemperaturen und bessere Kenntnisse über die Stratigraphie und Schneebedingungen können die Genauigkeit zukünftiger Simulationen steigern. Weitere Faktoren wie Schneeverwehungen und Straßenstaub, die zum besseren Verständnis der komplexen Prozesse der Entwicklung von polygonaler Tundra unter dem Einfluss von Infrastrukturen und Klimawandel beitragen, sollten in zukünftigen Untersuchungen berücksichtigt werden.

1 Introduction

Permafrost soils cover about 24% of the land mass in the Northern Hemisphere (Zhang et al., 1999). Climate warming has led to an increase in the mean global surface temperature of 0.87 ° C since the second half of the 19th century (IPCC, 2018). In the Arctic, this warming trend is three to four times as high as the global average (Serreze and Barry, 2011). This phenomenon, called Arctic amplification, is caused by the albedo feedback (i.e. the decline of sea ice cover and shortened snow cover period), the decreasing isolation of the ocean through the thinning sea ice, increasing cloud cover as well as changes in the oceanic and atmospheric circulation (Serreze and Barry, 2011). Rising air temperatures and snow cover changes are the most important climatic factors causing warming and thawing of permafrost (Goodrich, 1982). In Prudhoe Bay mean annual permafrost temperatures in a depth of 20m increased by 0.082°C per year in a period from 1978-2012 (Raynolds et al., 2014). Since the discovery of large natural resources and the subsequent construction of large-scale infrastructure that strongly modifies the thermal properties of the ground, human activities in the Arctic have become an additional important factor. This modification can lead to increased heat fluxes that enhance permafrost degradation (Stern and Gaden, 2015). The resulting ground ice melt leads to thaw subsidence and the formation of ponds and thermokarst lakes (Kokelj and Jorgenson, 2013). Through these partially self-initiated processes arctic infrastructures are particularly exposed to risks. Linear infrastructures such as roads and railways are among the most vulnerable, as they can change critical functions such as snow cover accumulation and water drainage over long distances. Primarily, the damming of meltwater can lead to particularly rapid and severe degradation of the permafrost by increasing ground temperatures through changes in the surface and subsurface energy balance (Langer et al., 2016). Walker et al. (2015) studied the changes and degradation phenomena of the polygonal tundra on Spine Road in the Arctic's largest industrial complex in Prudhoe Bay, Alaska over a period of 45 years. These investigations have shown a different degree of degradation depending on the side of the road with significantly delayed degradation on the northern side (Figure 1). To be able to explain the asymmetric degree of degradation found at the study site, climate warming, the main cause of permafrost degradation, must have been accelerated and intensified by previously mentioned factors south of the road.

The main objective of this bachelor thesis is to simulate ice-wedge polygonal tundra under different hydrological conditions caused by the dam effect of the one meter high gravel road using the new version of the CryoGrid 3 land surface model (Nitzbon et al., 2018). I hypothesize that the draining hydrological conditions led to later thermokarst development on the north side of the road while water-impoundment on the south side led to an earlier initiation of thermokarst. Furthermore, the model is tested towards snow cover density, a

critical parameter that influences the evolution of soil temperatures. Another objective is to show the applicability of the model to the study site in Prudhoe Bay, Alaska.

2 Study Site

The study site is located north of Lake Colleen at the Spine Road (N 70.22°, W 148.47°) in Deadhorse – an unincorporated community within the census-designated place Prudhoe Bay – in North Slope, Alaska (Figure 2). Deadhorse with its 25-50 permanent- and up to 3000 temporary inhabitants lies in the continuous permafrost zone with permafrost depths of about 600m (Jorgenson et al., 2008). The cold tundra climate with maritime influences leads to a mean annual air temperature (MAAT) of -11.1°C and an average annual precipitation of 102.6mm in the study area (Kanevskiy et al., 2017). In 2011 the mean annual ground surface temperature was about -3.2°C while the temperature 20m beneath the surface was measured at approximately -6°C (see Figure 2.9 by Walker et al. (2014)). The MAAT and ground surface temperatures in Deadhorse increased in the past decades. Between 1987 and 2011 Walker et al. (2014) measured a warming trend of approximately 3°C for air temperatures and 2°C for ground temperatures in 20m depth in Deadhorse. In addition to the air temperature and soil composition the snow depth and the duration of a closed snow cover are key determinants for the ground temperatures and permafrost conditions at a speci

fic site. A continuous snow cover that lasts from October until May is typical for the region (Zhang et al., 1996). The permafrost at the study site, that lies in an area of ice-wedge polygonal tundra is ice-rich with a high variability in volumetric ice content between the polygon center and troughs with the underlying ice wedges. This leads to a great vulnerability of the permafrost to degradation caused by melting ground ice, not only due to a changing climate, but also because of human activities. In the 1960s huge oil reservoirs were found in the Prudhoe Bay area. The Prudhoe Bay oilfield is the largest in the U.S. and was the first developed oilfield in the arctic (Raynolds et al., 2014). Supporting infrastructure has been built on a total area of 2600km² since 1968. Thus the industrial complex in Prudhoe Bay is the largest in the Arctic (Raynolds et al., 2014). Infrastructures affect the underlying permafrost in multiple ways. Increased heat transfer into the ground and accelerated permafrost thawing are to be expected for most infrastructures. Streets such as the Spine Road, which was constructed in 1969 and forms a one meter high dam, can severely affect the water runoff and alter the hydrology of the surrounding area, change the snow distribution by causing snow banks along its edges (with possibly higher snow depths on the leeward side) and lead to vegetation and albedo changes by covering the tundra with road dust (Walker et al., 2015). Intensive studies by Walker et al. (1980) and Walker et al. (2015) not only showed intensifying thermokarst development at the formerly intact polygonal tundra site where the Spine Road was built, but also described the diverging landscape changes on the different sides of the road. In 2014 the polygons on the south side of the road were mostly high-centered with an active layer thickness (ALT) of about 60cm, large and deep wet troughs and wet tundra vegetation. Compared to the north side where low-centered polygons, an ALT of approximately 50cm, shallow troughs and moist tundra vegetation were found, these are clear signs of greater degradation of the polygonal tundra south of Spine Road. Before the road was built in 1969, more wet tundra and thermokarst was found on the northern side (Walker et al., 2015).

3 Methods

3.1 CryoGrid 3 Land Surface Model

The one-dimensional CryoGrid 3 land surface model which was used to run the simulations for this thesis is able to simulate subsurface temperatures in permafrost regions by calculating the surface energy balance and the heat conduction equation with phase change (Westermann et al., 2016). Through the development of additional modules the model now includes a hydrology scheme, a lake module and an excess ice module with the capability to simulate soil subsidence. Nitzbon et al. (2018) applied CryoGrid 3 to the heterogeneous micro-topography of ice-wedge polygonal tundra using a tiling approach (Figure 4). Accordingly, three tiles – polygon centers, rims and a connected system of troughs – are distinguished in the model. Each of the tiles corresponds to a one-dimensional representation of the subsurface in this parallelized version of CryoGrid 3 (Figure 3). The model includes snow redistribution as well as lateral heat and water fluxes in the ground. To scale these fluxes the polygonal landscape was simplified to consist of equally-sized hexagons (Figure 4). Especially important for this thesis is the implemented external water reservoir with a constant water level in an adjustable altitude that is hydrologically connected to the troughs (Figure 3). Negative reservoir heights lead to drainage of the troughs whereas positive reservoir heights result in flooding of the troughs. For a more detailed model description see Nitzbon et al. (2018).

3.2 Model setup and simulations

3.2.1 Meteorological forcing

To set up and run the model an atmospheric forcing containing the required meteorological data (air temperature, humidity, air pressure, precipitation, wind speed and incoming long- and short-wave radiation) serves as the upper boundary condition. In this thesis ERA-Interim, a global reanalysis dataset with a 3-hourly resolution provided by the European Centre for Medium-Range Weather Forecast (ECMWF), is

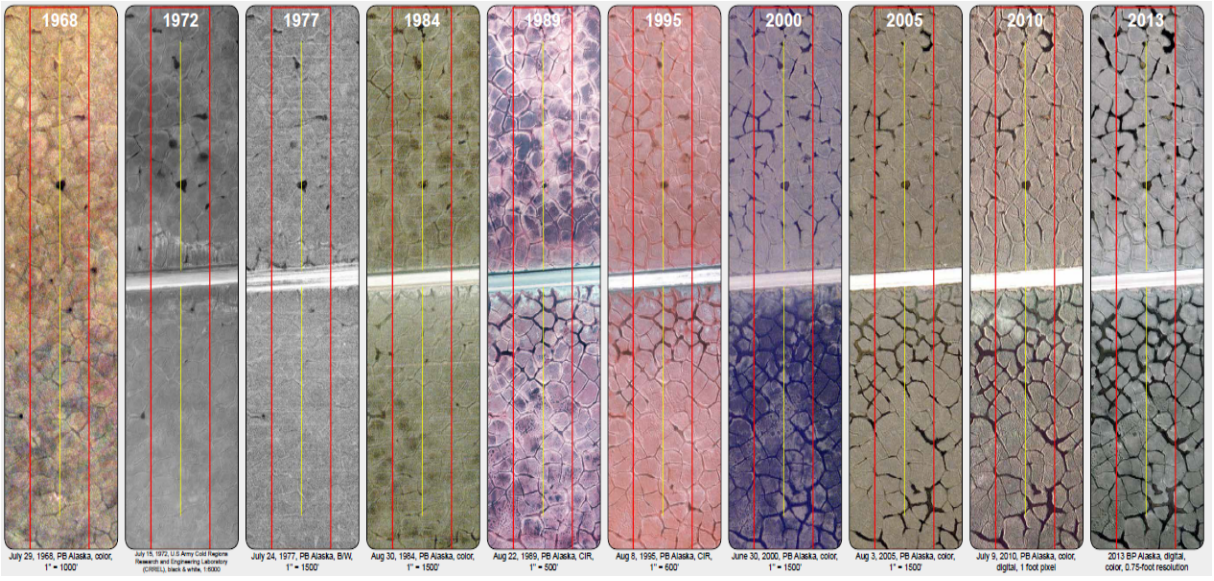

Figure 1. This figure by Walker et al. (2015) displays a time series of aerial images from 1968 to 2013 showing the evolution of ice-wedge polygonal tundra at Colleen Site A (see Figure 2) at Spine Road. The road was constructed in 1969 and therefore does not appear in the first image. The expansion of thermokarst development in 1989 indicates ice-wedge degradation in the troughs.

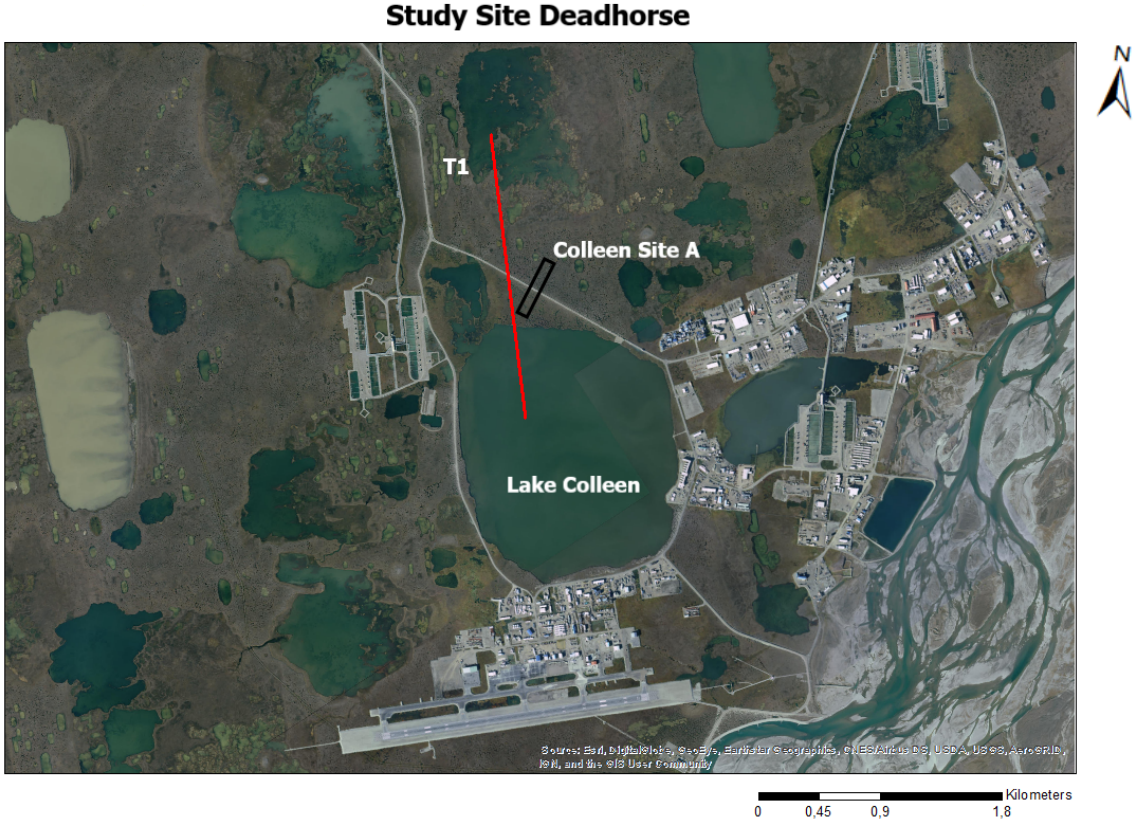

Figure 2. This figure shows the study site "Colleen Site A" by Walker et al. (2015) (see Figure 1 for a time series of aerial images of the study site) also investigated in this thesis and the elevation profile transect (T1) which is displayed in detail in Figure 5. The displayed map is a 60cm resolution World Imagery basemap by Esri (2018).

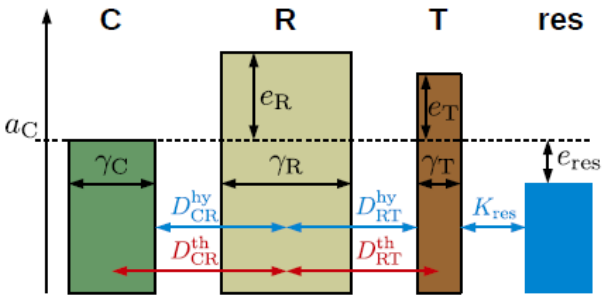

Figure 3. This figure by Nitzbon et al. (2018) displays the three tiles center (C), rim (R) and trough (T), the water reservoir (res) and the paramaters that define the topology and micro-topography. The micro-topography is specified by the elevations (e) relative to the center altitude (a_C) and the topology is displayed by the areal fractions (γ), the hydrological distances (D^{hy}) and the thermal distances (D^{th}). Through a hydraulic conductivity (K_{Res}) the trough-tile is hydrologically connected to the external reservoir with a fixed water level. A parallelized version of CryoGrid 3 was used so that eacht tile was simulated as a one-dimensional representation of the soil (Nitzbon et al., 2018).

utilized as the atmospheric forcing. It is based on a data assimilation system that includes extensive meteorological observations and a forecast model (Dee et al., 2011). The ERA-Interim product has a spatial resolution of approximately 80km and covers a time period from 1 January 1979 to mid-2018. Compared to the new higher-resolution ERA-5 dataset, that was only available from 2000 onwards when the simulations for this study were conducted, ERA-Interim was better suited for this work due to its extended time period. However, because of the relatively coarse spatial resolution of Era-Interim, about 75% of the grid cell (covering the area from N 70.875°, W 148.875° to N 70.125°, W 148.125°) that includes the study site (located at N 70.22°, W 148.47°) is covered by the Beaufort Sea. Since this grid cell is essentially a water cell, it was decided to use the meteorological forcing of the grid cell directly south of the study site to run the model (for a more detailed description see Appendix B1). The raw data from ERA-Interim is preprocessed to adapt the units and structure to CryoGrid3. Furthermore, a threshold temperature of 0.0°C was introduced in the pre-processing script, to prevent very rare ERA-Interim rainfall events below freezing temperatures and snowfall at temperatures higher than the threshold. Rainfall below the threshold temperature was added to snowfall, while snowfall above the threshold was added to rainfall.

3.2.2 Model parameters

To fit the model to the study site the microtopography (the tile-altitudes), the areal fractions of the tiles, the elevation of the external water reservoir (e_{res}) and the snow density were adjusted (Table A1). The altitudes of center (a_C), rim (a_R) and trough (a_T) were estimated to be a_C=13.3m, a_R=13.6m and a_T=13.5m respectively using Figure 9b and Figure 10 from Walker et al. (2015) and observations made by Everett and Parkinson (1977). The elevated rims and troughs are typical for mostly undisturbed low-centered polygonal tundra and assumed to be a good representation of the study site for the start of the simulations in 1979. The areal fractions of center (γ_C=0.55), rim (γ_R=0.35) and trough (γ_T=0.1) were approximated from measurements of well-developed 10m diameter low center polygons in the Prudhoe Bay area by Everett and Parkinson (1977) and from Figure 10 by Walker et al. (2015). Two different external water reservoir heights reflecting the different hydrological conditions on the north- and south side of the road were determined using the freely downloadable digital elevation model ArcticDEM Release 6 with a spatial resolution of 5m. A transect from Lake Colleen in the south to a partly drained thermokarst lake in the north of Spine Road (Figure 2) shows that the height difference between Lake Colleen and the tundra south of Spine Road is only about 0.2m while the external water reservoir lies about 1.7m below the tundra north of the road (Figure 5). Thus the external water reservoir height is set to e_{res}=-0.2m for the south side and e_{res}=-1.7m for the north side of the road relative to the altitude of the polygon center. This supports the hypothesis, that the one meter elevated Spine Road (Figure 5) forms a barrier for the water runoff from south to north. A specifically important but very uncertain parameter largely affecting the heat loss and cooling of the ground in winter is the snow density. To account for its uncertainty and to better understand the sensitivity of the model concerning this parameter, three different snow densities were chosen. Stuefer et al. (2014), Stuefer et al. (2012), Berezovskaya et al. (2010b), Berezovskaya et al. (2010a), Berezovskaya et al. (2008), Berezovskaya et al. (2007) and Kane et al. (2006) provide snow density data from in-situ measurements at the coastal plain of Arctic Alaska between 2006 and 2014. From the mean annual snow densities found at the coastal plain an average snow density (ρ_{snow}) of 264$\mathrm{kg\,m^{-3}}$ was calculated for the period covered by the measurements. Additionally lower snow densities of 250$\mathrm{kg\,m^{-3}}$ and 200$\mathrm{kg\,m^{-3}}$ used by Nitzbon et al. (2018) for a site in Siberia were tested in the simulations. Apart from the parameters mentioned, the model specifications remained unchanged (for a complete parameter list see Table 2 and Table D1 by Nitzbon et al. (2018)).

3.2.3 Soil stratigraphy

Based on sediment core analysis by Walker et al. (2015) as well as previous stratigraphies used for CryoGrid 3 model runs at polygonal tundra sites in Siberia by Nitzbon et al. (2018) and Westermann et al. (2016), the soil stratigraphy was adjusted to the study site (Table A2). Particularly important is the depth and amount of excess ground ice – a soil layer where the natural soil porosity (Φ_p) is exceeded

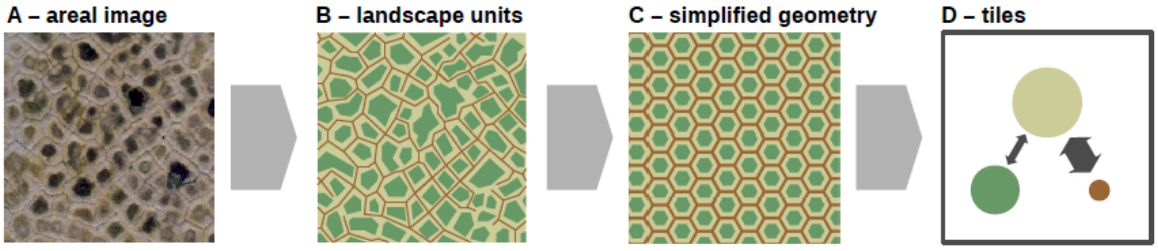

Figure 4. This figure by Nitzbon et al. (2018) displays the tiling approach used in this version of CryoGrid 3. The micro-topography of polygonal tundra is represented by three tiles (Centers (C), Rims (R) and Troughs (T)). The polygonal pattern found at tundra sites across the Arctic is simplyfied to a homogenous grid of equally-sized hexagons allowing the quantification of lateral fluxes and snow redistribution between the tiles (Nitzbon et al., 2018).

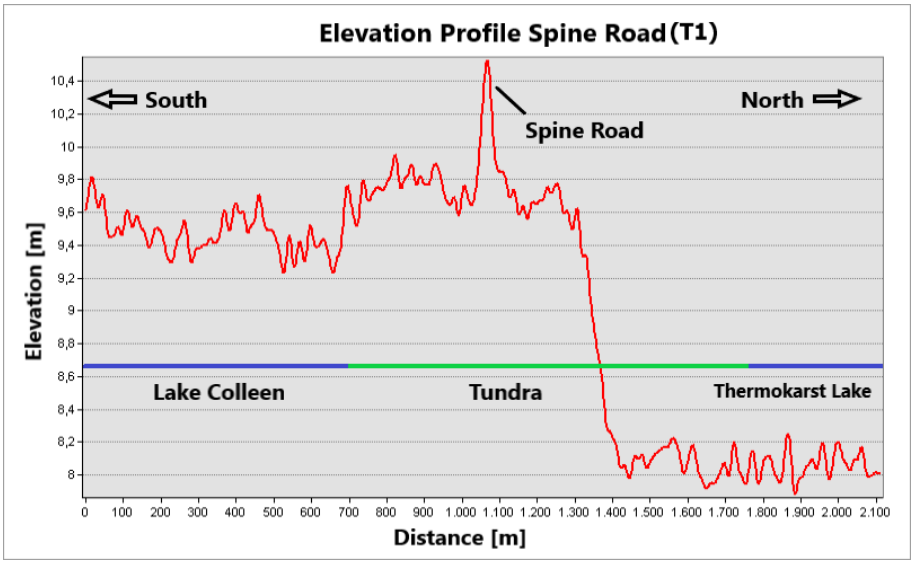

Figure 5. The chart displays the elevation profile of the transect T1 (see Figure 2). It was generated using the freely downloadable digital elevation model ArcticDEM Release 6 with a spatial resolution of 5m (see code and data availability) and reaches from Lake Colleen in the south to a partly drained thermokarst lake in the north of Spine Road. The lower altitude of the tundra in the direction of the drained thermokarst lake on the north side of the road and the one meter elevated Spine Road itself, stand out in this figure.

by the volumetric (frozen) water content (φ_w) – in the different tiles. The melting of this excess ice leads to soil subsidence and a change of the tundra microtopography (Liljedahl et al., 2016). Typically the largest amounts of ground ice in a polygonal tundra landscape can be found beneath the troughs where the ice wedges form. In Prudhoe Bay ice wedges are typically up to 5m thick and extend from about 0.5m to 5.5m depth (Walker and Everett (1991) and Figure 10 by Walker et al. (2015)). A volumetric excess ice content of 40% (φ_w=0.90 and Φ_p=0.50) was assumed for the ice wedges underlying a 10cm thick intermediate layer with 15% excess ice. At its top the ice wedges extend into the rims where an excess ice content of 10% was assumed from 0.7m depth downwards. For the polygon center the excess ice content was set to a small amount of 5% starting at a depth of 1m. At the top all three tiles were covered with a 15cm thick organic soil layer. This layer is especially important since the porose organic material, if dry, has an insulating effect on the soil. A mineral layer with a thickness of 85cm in the polygon center and only 35cm in the trough was placed between the organic rich soil at the top and the excess ice layer (Figure A3).

3.2.4 Temperature profile

In order to start the simulations at the study site, an initial temperature profile that is subdivided into polygon center, rim and trough, was generated for each of the different snow densities ρ_{snow}= 264kg m^{-3}, ρ_{snow}= 250kg m^{-3} and ρ_{snow}=

$200\,\mathrm{kg\,m^{-3}}$. To create these temperature profiles, borehole data by the Permafrost Laboratory (see code and data availability) in a depth from 4.3m to 53.3m that were conducted in 2006 at a site south of Deadhorse on the west side of Dalton Highway, was used to perform 30-year spin-up runs (see section 3.2.5 for a more detailed description). Figure 6 shows the borehole temperature profile from 2006 and the initial temperature profiles of the polygon centers for the year 1979 generated by the spin-up simulations.

3.2.5 Simulations

Three 30-year spin-up simulations for the three different snow cover densities (ρ_{snow}= $264\,\mathrm{kg\,m^{-3}}$, ρ_{snow}= $250\,\mathrm{kg\,m^{-3}}$ and ρ_{snow}= $200\,\mathrm{kg\,m^{-3}}$) and e_{res}=-1.7m were conducted to create an initial temperature profile for the start of the final runs. The lower external reservoir height of e_{res}=-1.7m that represents the hydrological conditions on the north side of the road is used for the spin-up since it is assumed that these conditions could be found at the study site prior to the construction of Spine Road. The spin-up runs cycled through the decade from 1979 to 1989 three times to adjust the model to the climatic conditions at the study site. After setting up the model as described in the previous sections, six simulations were performed for the period from October 1, 1979 to December 31, 2017. For each of the two external water reservoir heights, representing the different hydrological conditions of the north and the south side of the road, three model runs with the selected snow densities were conducted. These six model runs were repeated with a disabled excess ice module, to further analyze the influence of reservoir height and snow cover density on the ALT.

4 Results

4.1 Ground temperature profiles

As shown in Figure 6 the simulated ground temperatures significantly increased from 1979 to 2006 for all model runs. In a depth of 10-20m the ground temperatures under draining hydrological conditions on the northern side of Spine road (e_{res}=-1.7m) assuming a snow density of $264\,\mathrm{kg\,m^{-3}}$ were about 1°C warmer in 2006 than at the start of the simulation. During the 27-year period the ground temperatures south of the road (e_{res}=-0.2m, ρ_{snow}=$264\,\mathrm{kg\,m^{-3}}$) increased by approximately 1.5°C. Starting with 0.5°C warmer initial temperatures in a depth of 10-20m the temperature difference between the north and the south side of the road is even greater assuming a snow depth of $250\,\mathrm{kg\,m^{-3}}$. While the temperatures under draining hydrological conditions only increased by 1°C, the temperatures south of the road increased twice as much. The same trend with a temperature increase of up to 3.5°C applies to the model runs with a snow density of $200\,\mathrm{kg\,m^{-3}}$.

For depths of up to 15m the simulated temperature difference between different hydrological conditions is greater than between different snow densities. Below 15m, the temperature profiles of simulation-pairs with the same snow density approach each other, so that greater temperature differences are found for simulations with different snow densities (Figure 6).

The comparison of the borehole measurements with the simulated temperature profiles for the snow densities of ρ_{snow}=$264\,\mathrm{kg\,m^{-3}}$ and ρ_{snow}=$250\,\mathrm{kg\,m^{-3}}$ on the north side of Spine Road (e_{res}=-1.7m) in 2006 shows, that the simulated temperatures correspond to the measurements in the upper 15m with a deviation no greater than about 0.7°C. Below a depth of 15m the measured ground temperatures start to decrease after staying at a constant temperature of approximately -6.5°C between 10m and 20m depth, while the two simulations reach their minimum about 10m below the surface. In the upper 10m the simulated temperatures with a snow density of ρ_{snow}=$250\,\mathrm{kg\,m^{-3}}$ on the north side of the road and the simulation with a snow density of $264\,\mathrm{kg\,m^{-3}}$ on the south side very well match the borehole temperatures with a maximum deviation of about 0.2°C. From a depth of 20m the difference between the simulated temperatures and the measurements increases. In 50m depth the temperatures are 1.5°C warmer than the borehole temperatures.

The greatest deviations from the borehole temperatures are found for the model runs assuming a snow density of $200\,\mathrm{kg\,m^{-3}}$. While the simulated temperatures under draining hydrological conditions are about 3°C too warm at all depths, the modeled temperatures south of Spine Road exceed the measured temperatures by about 4-5°C (Figure 6).

4.2 Comparison between the ice-wedge degradation on the north and south side of Spine Road

The main objective of this bachelor thesis was the simulation of the ice-wedge degradation under different hydrological conditions caused by the dam effect of a one meter elevated gravel road. Figure 7 and Figure 8 show the evolution of the polygonal tundra during the entire simulation period from 1979-2017 assuming a snow density of $264\,\mathrm{kg\,m^{-3}}$ for an external water reservoir height of -0.2m on the south side and -1.7m on the north side of the road. During the first ten years the unsaturated low-centered polygons (LCP) on both sides of the road remain in a stable state with ALTs of about 40cm in the troughs, 50cm in the rims and 30-50cm in the polygon centers. The end-of-summer water table (WT) remains on a similar level as the ALT in the troughs and rims while the WT in the center is comparatively higher. Due to the lateral transport of snow from the elevated rims the average maximum SD is highest in the polygon centers with about 0.5m snow cover while SDs of 0.3m and 0.2m are typical for troughs and rims. Standing out from the previous years, the SD in 1989 is particularly high. In addition, the ALT in the troughs in 1989 for the first time exceeds a depth of 0.5m (Figure 7 and Figure 8). The resulting melt of excess

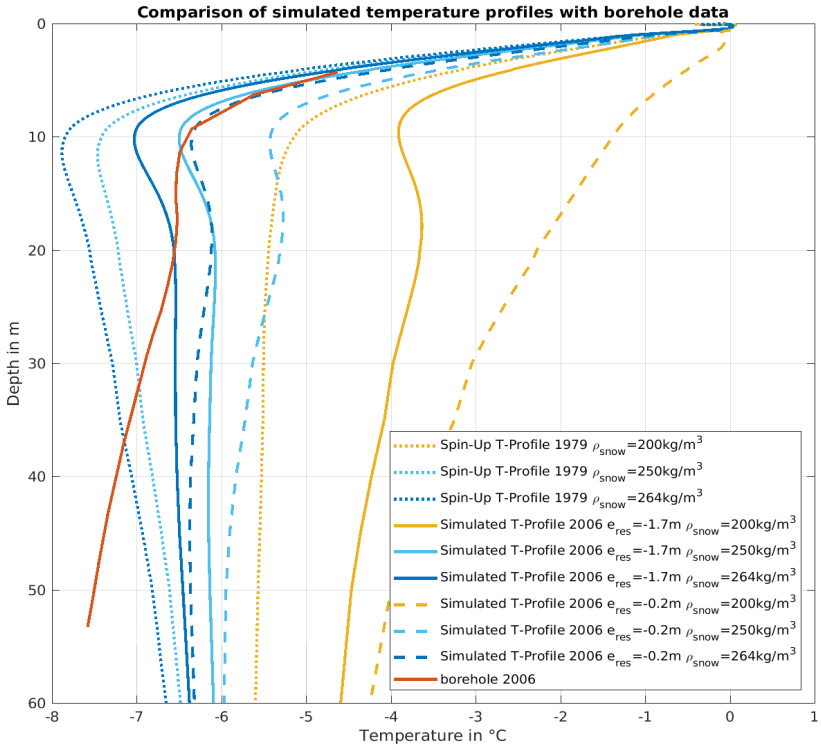

Figure 6. The figure displays the temperature profile measured in a borehole south of Deadhorse (red line), the spin-up temperature profiles of the three snow densities ρ_{snow}= 264kg m^{-3}, ρ_{snow}= 250kg m^{-3} and ρ_{snow}= 200kg m^{-3} in 1979, generated using the temperature data from the borehole, as well as the simulated temperature profiles on 1 october 2006 for each of the snow densities with the reservoir heights e_{res}=-1.7m and e_{res}=-0.2m.

ground ice leads to the first soil subsidence in the troughs. Until 1998 a period of slow subsidence of the troughs follows, reducing its altitude to that of the polygon centers (Figure A1). During this period the WT in the troughs increases until it reaches the ground surface in 1998 on the south side of the road and 1999 on the northern side. The further subsidence of the troughs in 1999 lead to a change from LCP to intermediate-centered polygons (ICP) where the rims are still elevated above the polygon centers while the troughs subside below the altitude of the centers. Besides the first subsidence of the rims, 1999 marks the start of a differing ice-wedge degradation on the different sides of the road. Reaching the level of the water reservoir, the troughs on the south side of the road experience an accelerated soil subsidence and thermokarst development with ponding water in the troughs between 1999 and 2011. Though, due to the development of an ice sheet in the water-filled troughs in winter, the SD on this side of the road remains stable at a typical snow cover height of about 50cm, while the SD north of the road increases with further subsidence reaching maximum annual SDs of more than 1m in the 2000s. The ALT in the rims steadily increases from 1999 onwards, reaching thicknesses of 1m and 1.3m in 2011 on the north and south side of the road, respectively. After 2011 the tundra on the south side stabilizes in a state which marks the transition from ICP to high-centered polygons (HCP) with equal altitudes of rims and polygon centers and 1.2m subsided troughs. North of the road the time period with a fast degradation of the ice wedges below the troughs only lasts until 2006 followed by a stabilization of the intermediate-centered polygonal tundra. The draining hydrological conditions on the north side of the road results in a decreased simulated soil subsidence of 0.9m in the troughs and 0.2m in the rims (Figure A1). The different degree of ice-wedge degradation on the two sides of the road ultimately resulting from warmer ground temperatures is very well reflected by the subsoil temperature differences of the simulations in 2006 described in 4.1. The simulations with snow densities of 250kg m^{-3} and 200kg m^{-3} found a similar evolution of the tundra with an increased degradation on the south side of Spine Road. Though the timing and and total amount of degradation differed from the simulation with ρ_{snow}=264kg m^{-3} (See section 4.2 and Appendix B2 for a more detailed description of the simulations with ρ_{snow}=250kg m^{-3} and ρ_{snow}=200kg m^{-3}).

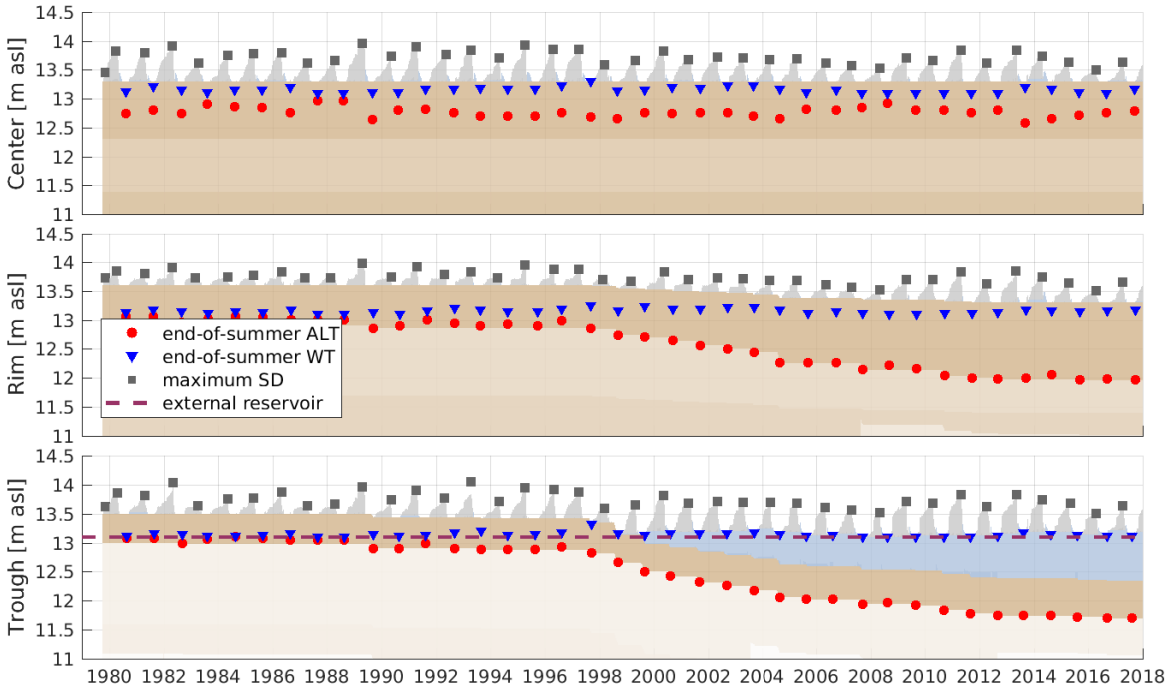

Figure 7. The figure shows the evolution of the polygonal tundra south of Spine Road (e_{res}=-0.2m) assuming a snow density of 264kg m^{-3} for the entire simulation period from 1979 to the end of 2017. It displays the snow depth (SD), the end-of-summer active layer thickness (ALT) and the end-of-summer water table (WT) for polygon center, rim and trough as well as the external reservoir height.

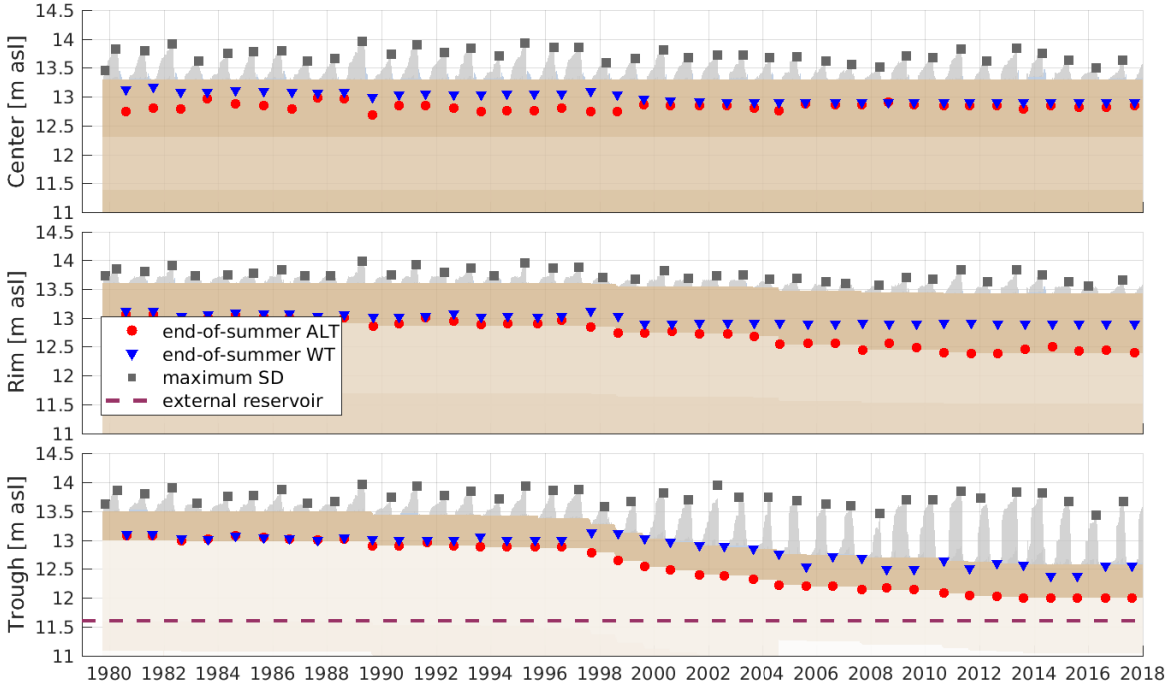

Figure 8. The figure shows the evolution of the polygonal tundra north of Spine Road (e_{res}=-1.7m) assuming a snow density of 264kg m^{-3} for the entire simulation period from 1979 to the end of 2017. It displays the snow depth (SD), the end-of-summer active layer thickness (ALT) and the end-of-summer water table (WT) for polygon center, rim and trough as well as the external reservoir height.

4.3 Sensitivity of the model to snow density

To better understand the sensitivity of the model to different snow conditions, simulations with snow densities of 264kg m^{-3}, 250kg m^{-3} and 200kg m^{-3} were conducted. These simulations revealed that the different snow densities which lead to a different snow cover insulation, affect the timing of ice-wedge degradation and subsequent soil subsidence. Figure 9 shows the subsidence of the troughs as an indicator for melting ice wedges for the six simulations. The timing of subsidence is very similar for the simulation-pairs with the same snow density. The period of fast soil subsidence with ρ_{snow}=200kg m^{-3} starts about 5-6 years earlier than the modeled ice-wedge degradation with ρ_{snow}=250kg m^{-3} and about 8 years earlier than the simulation with the highest snow density (ρ_{snow}=264kg m^{-3}). However, the rate of subsidence under different snow cover insulation is very similar during this period and amounts to about 10cm/year. The duration of the period with fast ice-wedge degradation and the resulting total amount of subsidence is dependend on the snow cover insulation and the side of the road (i.e. external water reservoir height). Under draining hydrological conditions the simulation with ρ_{snow}=264kg m^{-3} lead to a total subsidence of ∼0.9m, while the modeled subsidence with ρ_{snow}=250kg m^{-3} and ρ_{snow}=200kg m^{-3} amounts to 1m and 1.3m respectively. On the south side of the road (e_{res}=-0.2m) the total subsidence is increased by approximately 0.3m for ρ_{snow}=264kg m^{-3} and ρ_{snow}=250kg m^{-3}, while the system simulated with a snow density of 200kg m^{-3} did not reach a new equilibrium state until the end of the simulation period in 2017 and maintained a nearly constant rate of subsidence of about 10cm/year leading to a 2.2m difference of total subsidence between the two sides of the road (Figure 9). The different magnitude of ice-wedge degradation results in a different final state of the polygonal tundra. While the tundra on the south side of Spine Road assuming a snow density of 264kg m^{-3} stabilizes in a transitional state from ICP to HCP, the two simulations for snow densities of 250kg m^{-3} and 200kg m^{-3} result in a more severe change from LCPs to a high-centered polygonal tundra with a total soil subsidence in the troughs of 1.3m and 3.5m respectively (Figure A1 and Figure 9). As noted before, the year 1989 had a particularly great impact on the initial degradation of the tundra. That year a particularly strong soil subsidence in troughs occured in all model runs (Figure 9). Another winter standing out from the rest took place between 1982 and 1983. It initialized the first subsidence of three runs with a low snow density.

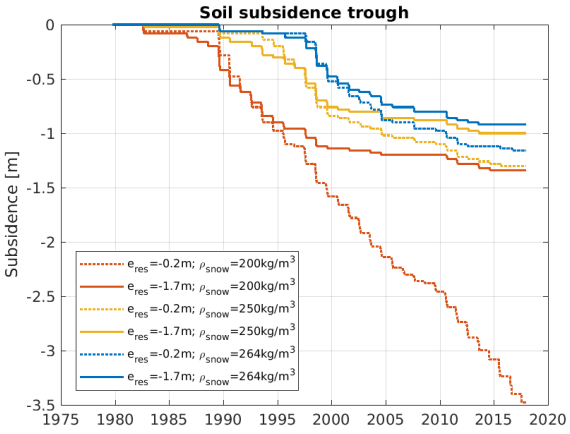

Figure 9. This chart displays the different magnitude of soil subsidence occuring in the troughs due to ice-wedge degradation for simulations with the two different external water reservoir heights (e_{res}=-1.7m and e_{res}=-0.2m) under different snow conditions (i.e. different snow densities ρ_{snow}= 264kg m^{-3}, ρ_{snow}= 250kg m^{-3} and ρ_{snow}= 200kg m^{-3}).

5 Discussion

5.1 Applicability of the model to the study site

The spin-up runs and the simulations with the enabled excess ice module show that the model is applicable to a tundra site in Alaska. In the upper 20m the initial temperature profiles generated by the spin-up for the year 1979 deviated by about ±1°C from borehole measurements in Deadhorse in 2006 with about 1°C decreased temperatures assuming snow densities of 264kg m^{-3} and 250kg m^{-3} and 1°C higher temperatures with ρ_{snow}=200kg m^{-3} (Figure 6). Due to the ground temperature rise triggered by climate warming, observed soil temperatures in a depth of 20m were about 2°C colder in 1979 than in 2006 (Raynolds et al., 2014). During this year the spin-up temperatures for ρ_{snow}=264kg m^{-3} and ρ_{snow}=250kg m^{-3} in 20m depth were only about 1°C and 0.7°C colder than the measured temperatures. This is due to the fact, that the warmer borehole temperatures from 2006 were used as an initial temperature profile for the spin-up runs cycling between 1979 and 1989. Particularly the simulated temperatures in depths below ∼20m are too warm, with simulated temperatures exceeding the measurements by approximately 1°C in a depth of 50m. To address this issue, it would be necessary to extrapolate the ground temperatures in the year 1979 based on the measurements in 2006 and warming trends for different depths. However, the model runs with the two higher snow densities (ρ_{snow}=264kg m^{-3} and ρ_{snow}=250kg m^{-3}) very well represent the ground temperatures in the study area in the upper 10m since the simulated temperatures for the hydrological conditions north of the road (e_{res}=-1.7m) in 2006 only differ by about 0.5°C from

the borehole measurements. As the main focus of this study lies on the simulation of ice-wedge degradation in the upper 5m of the ground, it was most important to well represent the temperatures in the upper soil layers. For future studies, however, an improved initial temperature profile should be determined.

Due to the heterogenity of the landscape there is a lot of uncertainty when comparing simulated SD and ALT with measurements. Though the modeled SDs of 0.3-0.7m in the polygon center were in close agreement with meteorological data from the airport in Deadhorse. Snow cover heights of 0.25-0.55m were found between 1997 and 2001 (Romanovsky et al., 2003). Measurements between 1987 and 1992 by Romanovsky and Osterkamp (1997) show that the ALT simulated with CryoGrid 3 was very accurate during this period. The measurements in Deadhorse indicated a particularly high ALT of about 0.65m for 1989 (see Figure 8 by Romanovsky and Osterkamp (1997)) which matches the modeled ALT in the polygon center which was at about 0.6m. The higher ground temperatures indicated by the high ALT in 1989 resulted in ice-wedge degradation in the troughs for all simulations (Figure 9).

Aerial images of the study site of Walker et al. (2015) show the first thermokarst development in 1989, during the same year, the first ice-wedge degradation was simulated for the model runs with ρ_{snow}=264$\mathrm{kg\,m^{-3}}$ and ρ_{snow}=250$\mathrm{kg\,m^{-3}}$ (Figure 1). The simulated stabilization of the tundra characterized by a slow down of ice-wedge degradation around 2005 is also reflected by the aerial images, which do not show major changes from 2000 onwards (Figure 1). Though, the comparison between the degradation phenomena on the aerial photographs and the simulated ice wedge degradation is difficult, since the the amount of soil subsidence which is used to describe the degree of degradation in the simulations, is not visible on the aerial photographs. The degradation on the aerial images can only be determined by looking at the amount of water ponding in the troughs. Moreover, the aerial images were taken at a specific date and do not reflect the condition of the tundra over an entire year. While water-filled troughs on the south side of Spine Road are apparent on the aerial photographs from 1989 onwards, the simulated water accumulation in the troughs south of the road starts almost a decade later for snow densities of ρ_{snow}=264$\mathrm{kg\,m^{-3}}$ and ρ_{snow}=250$\mathrm{kg\,m^{-3}}$ (Figures 7 and B2). In the simulation with ρ_{snow}=200$\mathrm{kg\,m^{-3}}$ ponding water in the troughs can be found from 1991 onwards (Figure B4).

The total soil subsidence in the troughs for all model runs with ρ_{snow}=264$\mathrm{kg\,m^{-3}}$ and ρ_{snow}=250$\mathrm{kg\,m^{-3}}$ ranged from 0.8m to 1.3m over the simulation period of 39 years. LiDAR measurements by Walker et al. (2015) show a maximum depth of the troughs of about 1.0m in the south and 0.7m north of Spine Road (Figure 9b by Walker et al. (2015)). These observations are best reflected in the simulations with a snow density of 264$\mathrm{kg\,m^{-3}}$ where the total subsidence in the troughs amounts to 1.2m south of the road and 0.9m on the northern side (Figure 9). Walker et al. (2015) found a degradation from LCP to HCP on the south side and a low-centered polygonal tundra north of the road in 2014. In agreement with the findings on the south side of Spine Road, the simulated ice-wedge degradation with CryoGrid 3 also led to a change from LCP to HCP (Figure A1). On the north side of the gravel road the simulated tundra degraded from LCP to an intermediate-centered polygonal tundra (Figure A1).

In summary, the soil temperatures from borehole measurements in the upper 10m and the subsidence-patterns were in close agreement with the model runs with snow densities of 264$\mathrm{kg\,m^{-3}}$ and 250$\mathrm{kg\,m^{-3}}$, while it is unclear whether the timing of the start of degradation is well represented in the simulations due to difficulties in the comparison with aerial images.

5.2 The impact of different snow- and hydrological conditions

Besides the air temperatures, snow conditions i.e. the snow density, SD and the timing and duration of the snow cover have one of the greatest impacts on the thermal regime of the ground in permafrost regions (Goodrich, 1982). The snow cover forms an insulating layer decreasing the heat loss of the ground in winter. A high SD and a low snow density increase the insulating effect of the snow (Zhang, 2005). The timing of the snow cover is also critical for the ground temperatures. While an early snowfall in autumn and an early snowmelt in spring lead to increasing ground temperatures during the subsequent summer season, late snowfall and snowmelt result in colder soil temperatures due to heat loss of the ground in autumn and insulation of the soil from warm air temperatures in spring (Ling and Zhang (2003); Stieglitz et al. (2003)). In agreement with the explained effects of snow conditions, simulations with lower snow densities and thereby greater SDs lead to higher ALT and earlier soil subsidence (Figure A2, Figure 9)). Due to the great impact of water bodies on ground temperatures, it was assumed that the water-filled troughs that develop on the south side of the road (Figures 7, B2 and B4) lead to earlier and more severe tundra degradation. Water bodies reduce the albedo and alter the surface and subsurface energy balance. Langer et al. (2016) found a five fold increase in subsurface heat gain triggered by shallow water bodies with 0.9m depth. Accordingly, simulations of polygonal tundra under different hydrological conditions in Siberia by Nitzbon et al. (2018) showed a strong influence of the hydrology on the timing of degradation. Soil subsidence with an external reservoir height of -1.0m started about two decades later than under wet conditions (e_{res}=0.0m). In contrast to these findings, in the simulations conducted in this study it appears, that the beginning of the subsidence is triggered by years of particularly heavy snowfall and is mostly dependent on the meteorological forcing, while the timing of the period with rapid degradation is dependend on the snow density. The height of the external water reservoir and the

resulting difference in hydrological conditions, on the other hand, affect the total amount of subsidence and the time it takes for the system to reach a new steady state. Furthermore, due to the increased insulating layer in winter and the earlier start of ice-wedge degradation, the total amount of simulated subsidence of the troughs was higher for lower snow densities (Figure 9).

5.3 Limitations of the model

Several assumptions and sparse data regarding snow conditions at the study site lead to different uncertainties. Following the assessment of aerial photos also studied by Raynolds et al. (2014), it was assumed that the LCP tundra was in a stable state on both sides of the road at the beginning of the simulations. Since Spine Road was already constructed one decade before the start of the simulation period it might be that changes not visible in the photos were already triggered by the gravel road. The microtopography of the polygonal tundra was simplified to be uniform for all polygons which allowed a perfect water runoff to the external water reservoir through the interconnected troughs. A more realistic scenario with a varying polygonal microtopography would not always allow drainage and lead to different degradation patterns.

The soil stratigraphy was approximated by looking at sediment core interpretations conducted by Walker et al. (2015). The depth of the excess ground ice layers also derived from these interpretations result in a particularly high uncertainty since different heights of these layers would affect the timing of the start of subsidence. By analyzing the ALT in the troughs of the simulations with a disabled excess ice module, preventing the subsidence of the soil, it is apparent that the first degradation and subsidence occurs when the active layer reaches the depth of the excess ice layer (Figure A2). The ice-wedge in the trough starts in a depth of 60cm. In the simulation with ρ_{snow}=200$\mathrm{kg\,m^{-3}}$ the active layer first reaches the depth of the ice wedge in 1982, triggering the first soil subsidence in 1983 (Figure 9). Similarly, the first soil subsidence for simulations with snow densities of 264$\mathrm{kg\,m^{-3}}$ and 250$\mathrm{kg\,m^{-3}}$ is found during the year in which the ALT for the first time exceeds 60cm. Due to the dependency of the start of degradation from the depth of the excess ice layer, lowering of the excess ground ice in the stratigraphy would result in a significantly delayed degradation.

The initial geometry and topography of the polygons was set up using available data and observations by Everett and Parkinson (1977) and Walker et al. (2015). Though, different initial elevations of rim and trough compared to the centertile would have lead to a change in the lateral fluxes and snow distribution.

The snow density which has proven to be a very important parameter for permafrost degradation was highly uncertain for the study site. It is strongly influenced by wind patterns and the microtopography. Furthermore, the snow density can vary substantially during one winter season and between different years, while it is a fix parameter in the model. Therefore the mean value of ρ_{snow}=264$\mathrm{kg\,m^{-3}}$ calculated from measurements across the coastal plain of northern alaska may differ significantly from the actual snow densities at the study site.

5.4 Further factors induced by the road

There are several factors not taken into account in this thesis which may have a significant impact on the evolution of the tundra at the study site. Snowdrifts alongside the road which are determined by the elevation and the slope of the road as well as wind direction and windspeed would lead to a higher SD and increased melt water. Thus a predominant northeast wind could lead to snowdrifts along the southern edge on the lee side of the road triggering an earlier and accelerated degradation of the tundra south of the road (see Appendix B3 for further thoughts on how to simulate snow drifts using CryoGrid 3). While the direct impact of the increased snow cover would only affect the immediate area along the road, meltwater runoff towards Lake Colleen (i.e. the external water reservoir) and the resulting waterlogging could affect areas further away from the road. This might be simulated by coupling two polygonal systems and routing water from one system into the other.

Besides changing the albedo, road dust can kill most of the vegetation adjacent to the road leading to a decreasing insulation in summer and an increasing ALT (Raynolds et al., 2014). Walker et al. (2015) found a several centimeters thick dust layer within the first 50m from Spine Road. The influence of this factor was not included in the simulations.

Furthermore, lateral influences of Lake Colleen resulting in erosion processes and progressing degradation of the tundra south of Spine Road were not taken into account in this bachelor thesis. If no drainage system is implemented, then further expansion of Lake Colleen is a growing risk and might ultimately result in road damage.

6 Conclusion

The CryoGrid 3 simulations that were conducted in this study could reproduce the different degree of ice-wedge degradation observed on the two sides of Spine Road. Though the simulations did not support the hypothesis that the different timing of ice-wedge degradation on the two sides of the road was caused by the different hydrological conditions resulting from the dam effect of the gravel road. While the total subsidence was related to the hydrology, different snow densities strongly influenced the timing of degradation. However, a different model setup, with a more representative initial temperature profile at all depths and an improved database of snow conditions and soil stratigraphy, could provide results that more accurately describe the evolution of the polygonal tundra at the study site. Further enhancements of the land

surface model like the implementation of a „road-tile“, the inclusion of the influence of wind direction and windspeed on the snow distribution and a dynamic vegetation module would allow for an improved representation of the polygonal tundra. Scheduled for 2019, the release of new ERA-5 data sets that will encompass the time period from 1950 onwards will enable simulations with higher spatial resolution that extend beyond the construction of Spine Road.

Code and data availability. The CryoGrid 3 model used in this thesis is available from https://github.com/CryoGrid/CryoGrid3/tree/xice_mpi_polygon_TC. The ERA-Interim data is downloadable from https://apps.ecmwf.int/datasets/data/interim-full-daily/levtype=sfc/. The 2m resolution ArcticDEM can be downloaded from http://data.pgc.umn.edu/elev/dem/setsm/ArcticDEM/mosaic/v3.0/2m/. The Esri "World Imagery" is available via https://www.arcgis.com/home/item.html?id=10df2279f9684e4a9f6a7f08febac2a9. Deadhorse borehole-data is available on the Permafrost Laboratory website: http://permafrost.gi.alaska.edu/site/dh1. The NCEP GFS data is downloadable from https://rda.ucar.edu/datasets/ds084.1/index.html#!access. The MATLAB scripts used to pre process the ERA-Interim data and to create figures used in this thesis are provided on the USB-Stick also containing the Bachelor thesis pdf file.

Acknowledgements. I want to thank my supervisor Dr. Moritz Langer for his support throughout this bachelor thesis. Through Your ideas and comments, as well as proofreading, I have learned a lot during this work. Furthermore, I would like to thank Jan Nitzbon for a lot of interesting talks, valuable comments and proofreading.

Appendix A: Tables and Figures

Table A1. The table shows the setup of the tile-altitudes (a_C, a_R and a_T), the areal fractions of center, rim and trough (f_C, f_R and f_T) and the external reservoir height (e_{res}). Furthermore, it displays the different values of the different snow densities (ρ_{snow}) used in the simulations.

Parameter	**Symbol**			**Unit**	**initial Value**		
	center	*rim*	*trough*		*center*	*rim*	*trough*
altitudes	a_C	a_R	a_T	m	13.3	13.6	13.5
areal fractions	γ_C	γ_R	γ_T	-	0.55	0.35	0.1
external reservoir height relative to a_C		e_{res}		m		-0.2, -1.7	
snow density		ρ_{snow}		$\mathrm{kg\,m^{-3}}$		200, 250, 264	

Table A2. The table shows the soil stratigraphy used for polygon center, rim and trough. The initial soil water content φ_w, the mineral content φ_m, the organic content φ_o and the natural soil porosity Φ_p are given as volumetric fractions. The depths are relative to the altitudes of center (a_C), rim (a_R) and trough (a_T).

Depth [m]	**Water φ_w**	**Mineral φ_m**	**Organic φ_o**	**Soil type**	**Natural porosity Φ_p**
Center (a_C=13.3m)					
0.00-0.15	0.65	0.05	0.10	sand	0.85
0.15-1.00	0.65	0.20	0.05	silt	0.75
1.00-5.30	0.55	0.40	0.05	sand	0.50
> 5.30	0.30	0.70	0.00	sand	0.30
Rim (a_R=13.6m)					
0.00-0.15	0.50	0.15	0.10	sand	0.75
0.15-0.70	0.65	0.30	0.05	silt	0.65
0.70-5.60	0.60	0.35	0.05	sand	0.50
> 5.60	0.30	0.70	0.00	sand	0.30
Trough (a_T=13.5m)					
0.00-0.15	0.50	0.10	0.15	sand	0.75
0.15-0.50	0.65	0.30	0.05	silt	0.65
0.50-0.60	0.65	0.25	0.10	sand	0.50
0.60-5.50	0.90	0.05	0.05	sand	0.50
>5.50	0.30	0.70	0.00	sand	0.30

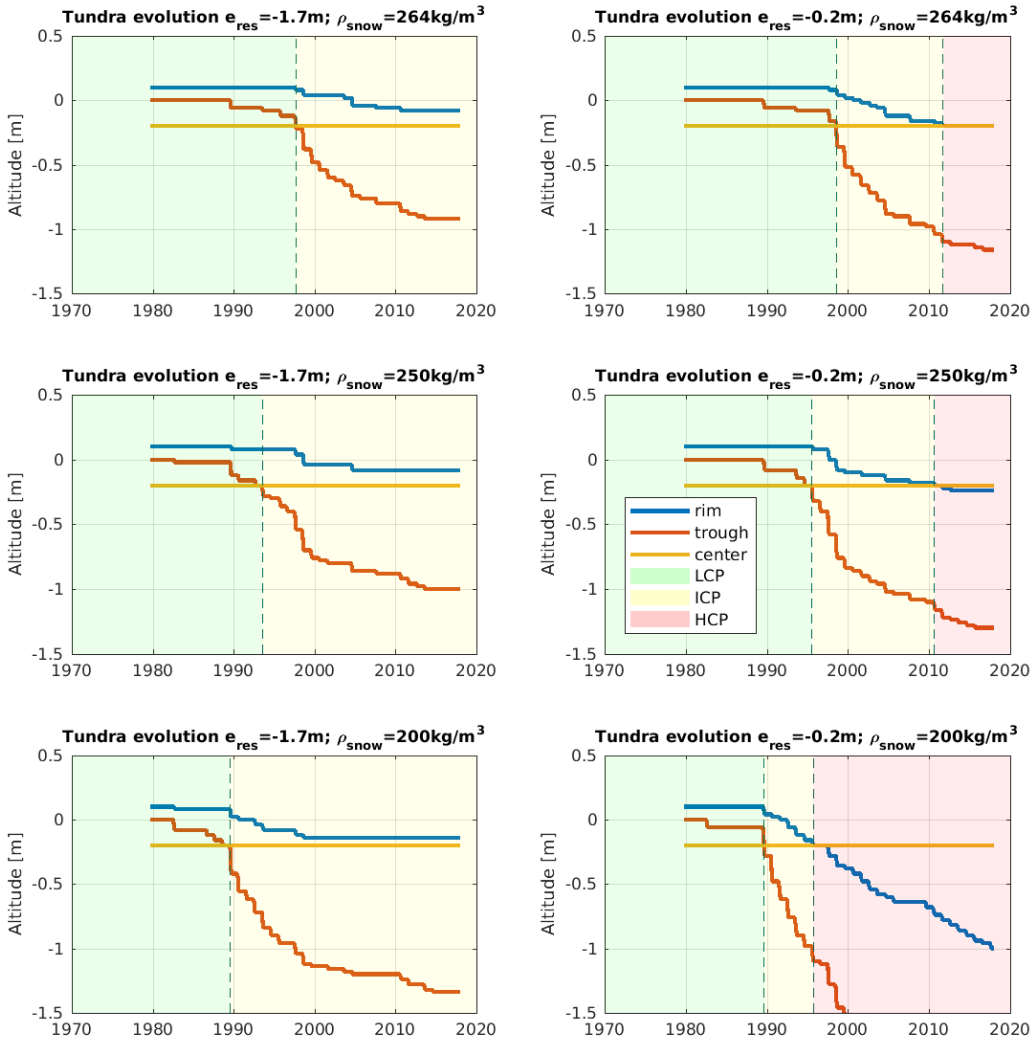

Figure A1. The figure displays the soil subsidence occuring in center rim and trough and the resulting evolution from low-centerd polygons (LCP) to intermediate-centered polygons (ICP) and high-centered polygons (HCP) during the entire simulation period (1979-2017) for the simulations with enabled excess ice module. The six charts included in this figure are splitted into two columns representing the two sides of Spine Road. On the left side the simulations for the south side of the road (e_{res}=-0.2m) with different snow densities (ρ_{snow}=264kg m^{-3}, ρ_{snow}=250kg m^{-3} and ρ_{snow}=200kg m^{-3}) are shown, while the simulations for the north side of Spine Road (e_{res}=-1.7m) are displayed in the right column.

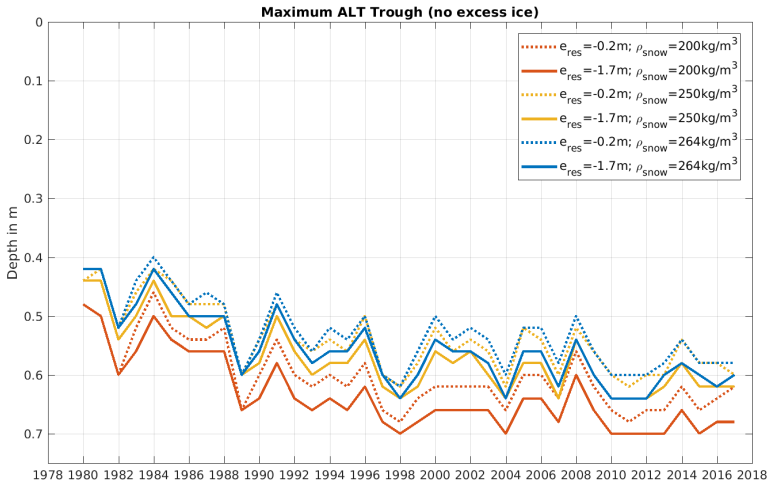

Figure A2. The chart displays the annual maximum active layer thickness (ALT) for the simulations on both sides of Spine Road (e_{res}=-1.7m and e_{res}=-0.2m) assuming different snow densities (ρ_{snow}=264kg m^{-3}, ρ_{snow}=250kg m^{-3} and ρ_{snow}=200kg m^{-3}) with a disabled excess ice module during the simulation period from 1979 to 2017.

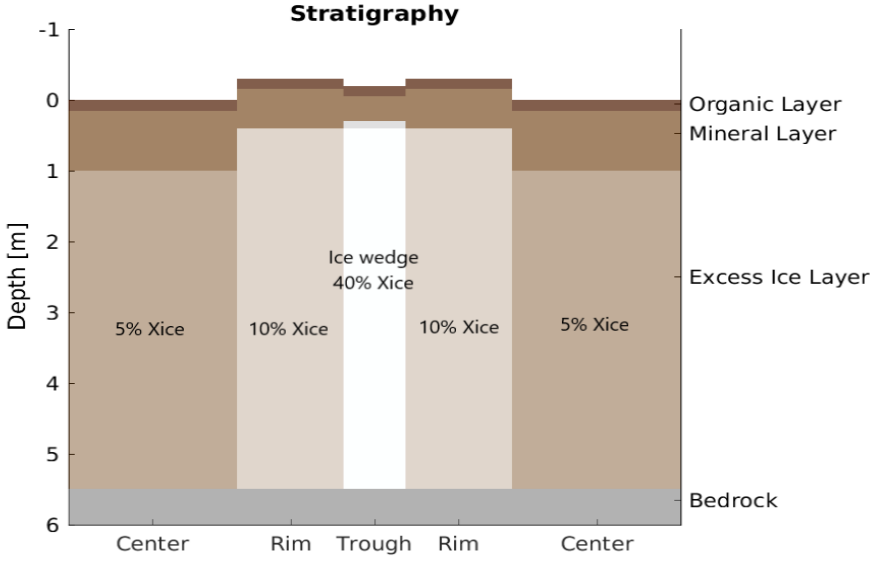

Figure A3. The figure displays the stratigraphy used for the simulations through a cross-section of one ice wedge and the surrounding polygon rims and centers. Higher volumetric excess ice (Xice) is displayed using lighter colors.

Appendix B: Supplement

B1 Meteorological forcing

In this section the air temperatures from the ERA-Interim grid cell at the coast (covering the area from N 70.875°, W 148.875° to N 70.125°, W 148.125°), the ERA-Interim grid cell directly south to the coastal cell (N 70.125°, W 148.875° to N 69.375°, W 148.125°) and the air temperatures provided by the Global Forecast System (GFS) of the National Centers for Environmental Predictions (NCEP) are compared. Just like ERA-Interim, the GFS is a reanalysis product that is based on measurements and a forecast model. It is available from 15 January 2015 onwards and has a spatial resolution of 0.25° ((NCEP, 2015)). Figure B1 displays the air temperatures in the year 2016 provided by the three meteorological forcings. While the annual temperature amplitudes of the southern ERA-Interim grid cell (Land Grid Cell) and the GFS match each other, except for some peaks in the GFS data in winter and summer, the temperature amplitude of the northern ERA-Interim grid cell is about 10-20°C lower. Due to the great heat capacity of the sea that covers about 75% of the grid cell resulting in lower air temperatures in summer and warmer winter temperatures (see red circles in Figure B1) the temperature amplitude is decreased. Since the GFS data has a much higher spatial resolution and the grid cell that includes the study site in Deadhorse is a land cell, the air temperature data from the GFS is considered as a reference. Due to the close agreement of the southern ERA-Interim grid cell with the reference values, it was selected for the meteorological forcing in this bachelor thesis. An in-depth analysis of the differences between the two ERA-Interim grid cells regarding all other meteorological parameters used to run CryoGrid 3 (rainfall, snowfall, specific humidity, long- and short wave radiation and sensible- and latent heat fluxes) would lead to an even more informed decision regarding the selection of the grid cell.

B2 The evolution of polygonal tundra

The simulated polygonal tundra at the two sides of the road, represented by the external reservoir heights of e_{res}=-0.2m (southern side of Spine Road) and e_{res}=-1.7m assuming a snow density of ρ_{snow}=250$\mathrm{kg\,m^{-3}}$ just like the model run with ρ_{snow}=264$\mathrm{kg\,m^{-3}}$ starts in a stable condition with low-centered polygons. From 1979 to 1989 the tundra remains in a stable state (Figure B2 and Figure B3). Due to the lower snow density, the SDs are a few centimeters higher. Until 1989, where the first ice-wedge degradation starts, the ALTs and WTs for center, rim and trough are the same as in the simulations with ρ_{snow}=264$\mathrm{kg\,m^{-3}}$ (see section 4.2). While the ice wedges in the model run with the highest snow density (ρ_{snow}=264$\mathrm{kg\,m^{-3}}$) remain stable between the initial degradation in 1989 and 1998, the ice-wedges in this simulations (ρ_{snow}=250$\mathrm{kg\,m^{-3}}$) keep degrading from 1989 onwards (Figure B2 and Figure B3). The ice wedges on the north side of Spine Road degrade slightly faster until 1993 (Figure 9. In 1997 the WT on the south side of the road reaches the surface and water begins to accumulate in the troughs. From this year onwards the total subsidence south of Spine Road exceeds the subsidence resulting from ice-wedge degradation on the northern side. While the snow depth on the north side of the road keeps increasing throughout the the entire period with increasing subsidence, the snow depth south of Spine Road only increases until the soil subsided to the height of the external water reservoir 20cm below the polygon center altitude. From this point, the snow depth stabilizes at typical snow cover heights of 50cm, since the snow cover is building up on the frozen water that accumulates in the troughs. Under the draining hydrological conditions on the north side of Spine Road, the snow cover in the troughs reaches heights of more than 1m (Figure B2 and Figure B3). From 2000 the tundra north of Spine road starts to stabilize, while the soil subsidence on the southern side of the road remains at a slow rate of about 3cm/year. The total subsidence in the troughs for the simulations with ρ_{snow}=250$\mathrm{kg\,m^{-3}}$ during the entire simulation period amounts to 1m for the draining hydrological conditions north of Spine Road and 1.3m south of the gravel road for the simulations with (Figure 9).

The simulations of the tundra with a low snow density of 200$\mathrm{kg\,m^{-3}}$ result in the most severe ice-wedge degradation during the simulation period. While the system in the model runs with the higher snow densities remain stable for the first decade, the ice-wedge degradation in the troughs starts in 1983 on both sides of the road under the ρ_{snow}=200$\mathrm{kg\,m^{-3}}$ scenario. The lower snow density leads to an increased insulating layer with about 10cm higher SDs. As seen in Figure 6, the initial ground temperatures after the spin-up runs were significantly warmer for a snow density of 200$\mathrm{kg\,m^{-3}}$. The ALT in the troughs exceeds 50cm in 1983 leading to the first ice-wedge degradation and soil subsidence. Until 1989 a phase of slow degradation with a subsidence rate of about 3cm/year follows (Figure 9). In 1989, the year in which the other simulations (ρ_{snow}=264$\mathrm{kg\,m^{-3}}$ and ρ_{snow}=250$\mathrm{kg\,m^{-3}}$) experienced the first degradation, an ALT of more than 70cm results in the first subsidence of the rims. Furthermore, in 1989 the phase of fast degradation with a subsidence rate of about 10cm/year starts. Water begins to accumulate in the troughs on the south side of the road from 1991 onwards. On the north side of Spine Road the phase of fast subsidence only lasts until 1995, while the subsidence rate south of the gravel road remains at the 10cm/year until the end of the simulation period (Figure 9). Between 1995 and 2000 the ice-wedge degradation north of Spine Road slows down, resulting in a subsidence rate of about 2cm/year. From the year 2000, the tundra north of the road start to stabilize in a state of ICP and a total subsidence of 1.3m (Figure A1). The simulation of the tundra south of Spine Road assuming a snow

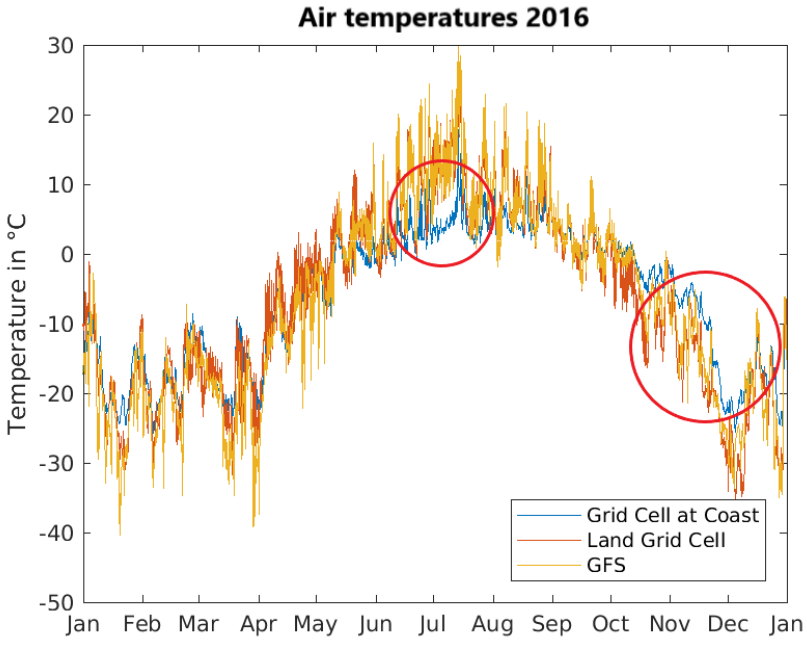

Figure B1. In this figure the 2016 air temperature data of the two meteorological forcings by ERA-Interim are compared to the NCEP GFS data in Deadhorse. The ERA interim forcing data differs due to the selected grid cell. The meteorological data of the southern grid cell (Land Grid Cell) provided by ERA-Interim is used as the meteorological forcing for the simulation in this bachelor thesis. The red circles mark interesting differences in the air temperatures of the different forcings (see Appendix B1 for a detailed description).

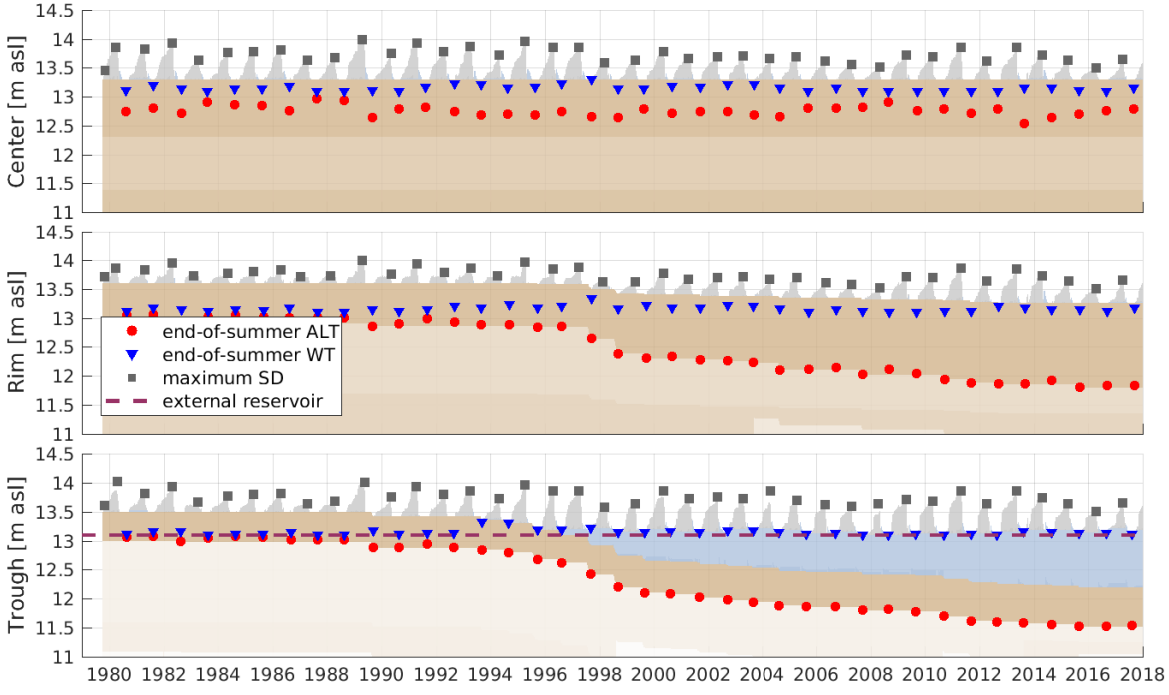

Figure B2. The figure shows the evolution of the polygonal tundra north of Spine Road (e_{res}=-0.2m) assuming a snow density of 250kg m^{-3} for the entire simulation period from 1979 to the end of 2017. It displays the snow depth (SD), the end-of-summer active layer thickness (ALT) and the end-of-summer water table (WT) for polygon center, rim and trough as well as the external reservoir height.

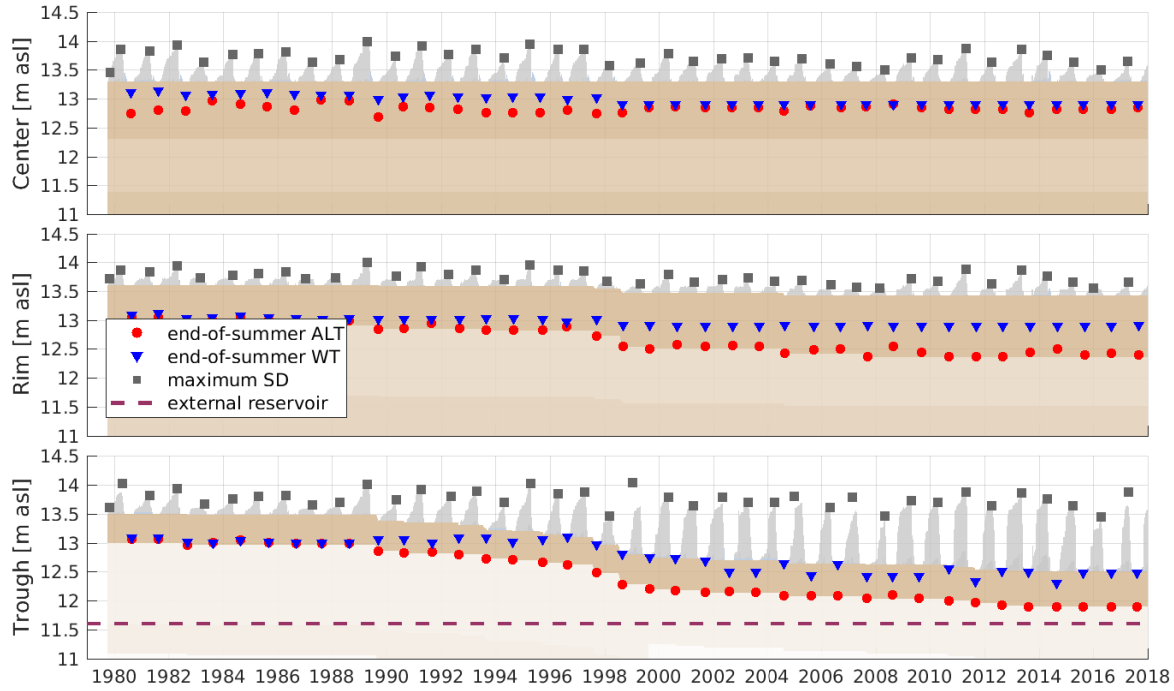

Figure B3. The figure shows the evolution of the polygonal tundra north of Spine Road (e_{res}=-1.7m) assuming a snow density of 250kg m^{-3} for the entire simulation period from 1979 to the end of 2017. It displays the snow depth (SD), the end-of-summer active layer thickness (ALT) and the end-of-summer water table (WT) for polygon center, rim and trough as well as the external reservoir height.

density of 200kg m^{-3} is the only model run, where the tundra does not reach a new equilibrium state. The total soil subsidence occuring in the troughs amounts to about 3.5m in 2017 (Figure 9). This simulation results in the greatest difference in the degree of degradation between the two sides of the road.

B3 Simulating the impact of snow drifts

The objective of this bachelor thesis to simulate the ice-wedge degradation along a gravel road in Prudhoe Bay and to better understand the impact of the infrastructure on the surrounding tundra did not change during the work on this subject. Due to the variety of impacts (i.e. change of snow distribution, water drainage, vegetation) the road might have on the sensitive permafrost landscape, there were different ideas regarding the specific setup of the model and the simulations. At the beginning, the impact of the one meter elevated road on the snow distribution seemed to be the most interesting. Snow drifts forming along the edges of the road could lead to an accelerated and more severe ice-wedge degradation due to the increased insulation of the soil in winter and increased melt water runoff in spring. Observations by Walker et al. (2015) showed an earlier degradation on the south side of Spine Road leading to the hypothesis, that snow drifts along the southern edge of the road could have accelerated the degradation. Since the meteorological forcing was almost done at this stage of the work on this thesis, the idea was to first check the main wind direction during the whole year and especially the prevailing wind direction in winter to see whether snow drifts would form south of the road rather than on the north side.

Two different approaches were discussed on how to represent the snow accumulation on one side of the road. The simple approach would be to scale up the snowfall from the forcing by raising the parameter „snow fraction“ in the model above 1. The difficulty using this approach is to estimate how much the snowfall should be increased to have a good representation of a snow drift. However, several simulations with different amounts of snow could be performed. This would also allow to test the sensitivity of the model to different snow depths.

The second more difficult approach would be to model the formation of a snow drift by implementing a new „road-tile“ and calculating the wind profile and the resulting snow accumulation in the lee of the elevated road. Furthermore, the new tile that would represent the road would need to be laterally connected to the three existing tiles (center, rim and trough) to enable lateral snow redistribution and lateral water and heat fluxes. Since the implementation of these new features would likely take too long for the three months period of a bachelor thesis, the first approach was selected to simulate the impact of different snow depths on the degradation of polygonal tundra.

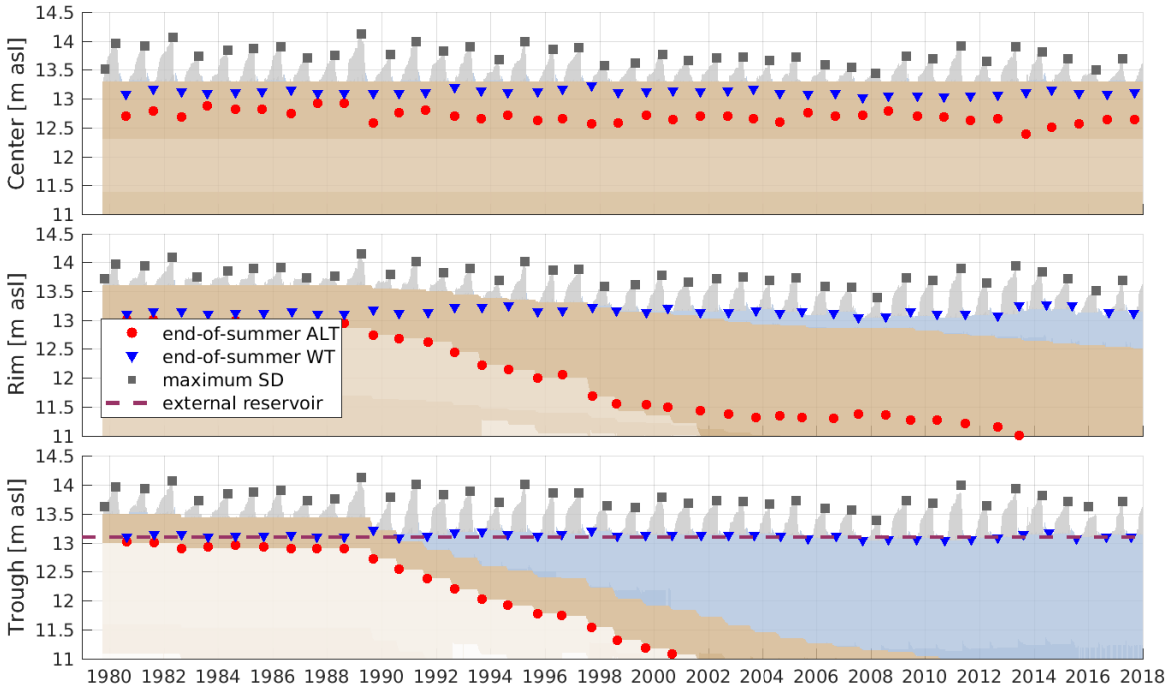

Figure B4. The figure shows the evolution of the polygonal tundra north of Spine Road (e_{res}=-0.2m) assuming a snow density of 200kg m^{-3} for the entire simulation period from 1979 to the end of 2017. It displays the snow depth (SD), the end-of-summer active layer thickness (ALT) and the end-of-summer water table (WT) for polygon center, rim and trough as well as the external reservoir height.

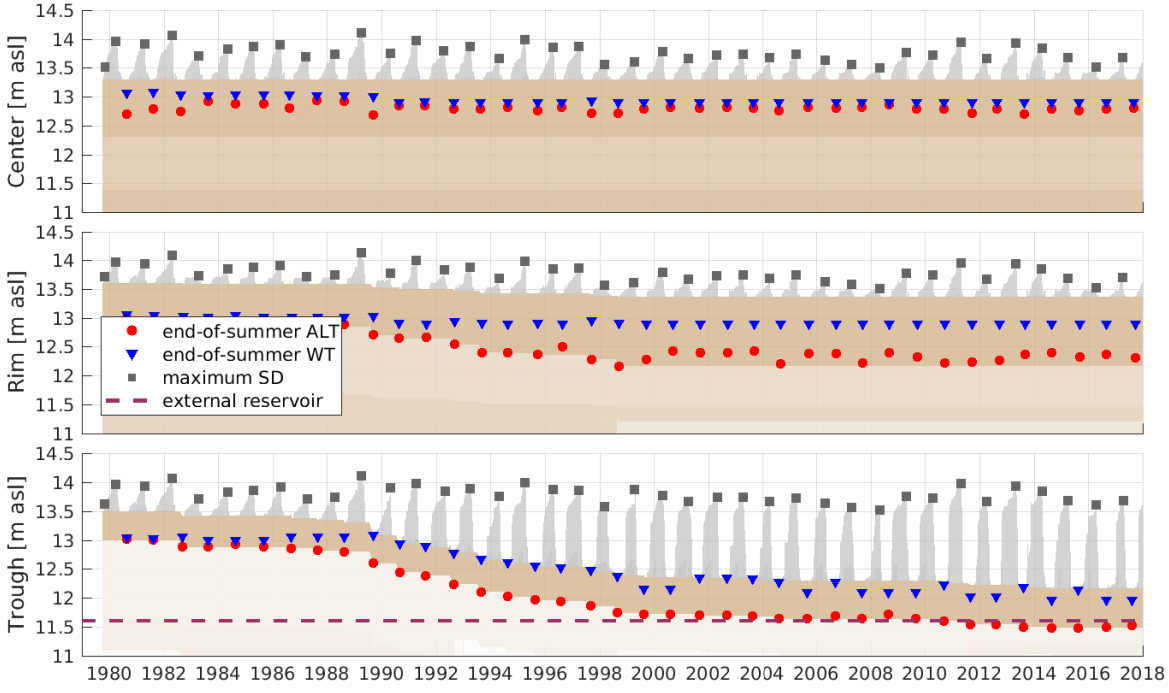

Figure B5. The figure shows the evolution of the polygonal tundra north of Spine Road (e_{res}=-1.7m) assuming a snow density of 200kg m^{-3} for the entire simulation period from 1979 to the end of 2017. It displays the snow depth (SD), the end-of-summer active layer thickness (ALT) and the end-of-summer water table (WT) for polygon center, rim and trough as well as the external reservoir height.

While starting to set up the model (i.e. generating initial temperature profiles, set up a representative stratigraphy) I looked for areial images showing snow dirfts along Spine road. Due to the high spatial resoltion needed to identify features like snow drifts, frequent cloud cover and the short time period in which snow drifts could be observed, the data base was very sparse. In fact, no snowdrifts could be detected on the aerial images.

Though high-resolution aerial images (Figure 1) brought another influencing factor into focus. Due to its elevation and a similar active layer thickness compared to the surrounding tundra, the road forms a partly frozen barrier and possibly prevents water drainage from the south- to the north side of the road (see Figure 9b by Walker et al. (2015)). The reduced meltwater runoff could lead to ponding water that changes the albedo, heat capacity and conductivity (for further explanaitions of the effect of ponding water on permafrost see 5.2). Due to the lack of evidence of snowdrifts on aerial images and the interesting hypothesis regarding the impact of the road on the hydrology and timing of the degradation of the polygonal tundra, I decided to simulate the influence of different hydrological conditions on the tundra at Spine Road. However, the idea of simulating snowdrifts as described above was not discarded but postponed. Modeling the influence of snowdrifts could be combined with the simulations performed in the bachelor thesis to provide a more detailed description of the evolution of the polygonal tundra under the influence of an elevated gravel road.

References

Berezovskaya, S., Derry, J., Kane, D., Gieck, R., Lilly, M., and White, D.: Snow survey data for the Kuparuk Foothills Hydrology Study: Spring 2007. July 2007, University of Alaska Fairbanks, Water and Environmental Research Center, Report INE/WERC, 7, 21, 2007.

Berezovskaya, S., Derry, J., Kane, D., Geick, R., Lilly, M., and White, D.: Snow survey data for the Kuparuk foothills hydrology study: Spring 2008, University of Alaska Fairbanks, Water and Environmental Research Center, Report INE/WERC, 8, 40, 2008.

Berezovskaya, S., Derry, J., Kane, D., Gieck, R., and Lilly, M.: Snow survey data for the central North Slope watersheds: Spring 2009, University of Alaska Fairbanks, Water and Environmental Research Center, Report INE/WERC, 10, 2010a.

Berezovskaya, S., Hilton, K., Derry, J., Youcha, E., Kane, D., Gieck, R., Homan, J., and Lilly, M.: Snow survey data for the central North Slope watersheds: Spring 2010, University of Alaska Fairbanks, Water and Environmental Research Center, Report INE/WERC, 10, 2010b.

Dee, D. P., Uppala, S. M., Simmons, A. J., Berrisford, P., Poli, P., Kobayashi, S., Andrae, U., Balmaseda, M. A., Balsamo, G., Bauer, P., Bechtold, P., Beljaars, A. C. M., van de Berg, L., Bidlot, J., Bormann, N., Delsol, C., Dragani, R., Fuentes, M., Geer, A. J., Haimberger, L., Healy, S. B., Hersbach, H., Hólm, E. V., Isaksen, L., Kallberg, P., Köhler, M., Matricardi, M., McNally, A. P., Monge-Sanz, B. M., Morcrette, J.-J., Park, B.-K., Peubey, C., de Rosnay, P., Tavolato, C., Thépaut, J.-N., and Vitart, F.: The ERA-Interim reanalysis: configuration and performance of the data assimilation system, Quarterly Journal of the Royal Meteorological Society, 137, 553–597, https://doi.org/10.1002/qj.828, https://rmets.onlinelibrary.wiley.com/doi/abs/10.1002/qj.828, 2011.

Esri: "World Imagery" basemap. 20.12.2018 10:37, https://www.arcgis.com/home/item.html?id=10df2279f9684e4a9f6a7f08febac2a9, 2018.

Everett, K. R. and Parkinson, R. J.: Soil and Landform Associations, Prudhoe Bay Area, Alaska, Arctic and Alpine Research, 9, 1–19, https://doi.org/10.1080/00040851.1977.12003897, 1977.

Goodrich, L. E.: The influence of snow cover on the ground thermal regime, Canadian Geotechnical Journal, 19, 421–432, https://doi.org/10.1139/t82-047, 1982.

IPCC: Summary for Policymakers. In: Global warming of 1.5°C. An IPCC Special Report on the impacts of global warming of 1.5°C above pre-industrial levels and related global greenhouse gas emission pathways, in the context of strengthening the global response to the threat of climate change, sustainable development, and efforts to eradicate poverty [V. Masson-Delmotte, P. Zhai, H. O. Pörtner, D. Roberts, J. Skea, P. R. Shukla, A. Pirani, W. Moufouma-Okia, C. Péan, R. Pidcock, S. Connors, J. B. R. Matthews, Y. Chen, X. Zhou, M. I. Gomis, E. Lonnoy, T. Maycock, M. Tignor, T. Waterfield (eds.)]., p. 32 pp., 2018.

Jorgenson, M., Yoshikawa, K., Kanevskiy, M., Shur, Y., Romanovsky, V., Marchenko, S., Grosse, G., Brown, J., and Jones, B.: Permafrost characteristics of Alaska, 2008.

Kane, D., Berezovskaya, S., Irving, K., Busey, R., Geick, R., Chambers, M., Blackburn, A., and Lilly, M.: Snow survey data for the Kuparuk Foothills Hydrology Study: Spring 2006. July 2006, University of Alaska Fairbanks, Water and Environmental Research Center, Report INE/WERC, pp. 06–06, 2006.

Kanevskiy, M., Shur, Y., Jorgenson, T., R.N. Brown, D., Moskalenko, N., Brown, J., Walker, D., K. Raynolds, M., and Buchhorn, M.: Degradation and stabilization of ice wedges: Implications for assessing risk of thermokarst in northern Alaska, Geomorphology, 297, https://doi.org/10.1016/j.geomorph.2017.09.001, 2017.

Kokelj, S. and Jorgenson, M.: Advances in Thermokarst Research, Permafrost and Periglacial Processes, 24, 108–119, https://doi.org/10.1002/ppp.1779, 2013.

Langer, M., Westermann, S., Boike, J., Kirillin, G., Grosse, G., Peng, S., and Krinner, G.: Rapid degradation of permafrost underneath waterbodies in tundra landscapes—Toward a representation of thermokarst in land surface models, Journal of Geophysical Research: Earth Surface, 121, 2446–2470, https://doi.org/10.1002/2016JF003956, 2016.

Liljedahl, A. K., Boike, J., Daanen, R. P., Fedorov, A. N., Frost, G. V., Grosse, G., Hinzman, L. D., Iijma, Y., Jorgenson, J. C., Matveyeva, N., Necsoiu, M., Raynolds, M. K., Romanovsky, V. E., Schulla, J., Tape, K. D., Walker, D. A., Wilson, C. J., Yabuki, H., and Zona, D.: Pan-Arctic ice-wedge degradation in warming permafrost and its influence on tundra hydrology, Nature Geoscience, 9, 312, 2016.

Ling, F. and Zhang, T.: Impact of the timing and duration of seasonal snow cover on the active layer and permafrost in the Alaskan Arctic, Permafrost and Periglacial Processes, 14, 141–150, https://doi.org/10.1002/ppp.445, 2003.

NCEP: NCEP GFS 0.25 Degree Global Forecast Grids Historical Archive, https://doi.org/10.5065/D65D8PWK, 2015.

Nitzbon, J., Langer, M., Westermann, S., Martin, L., Aas, K., and Boike, J.: Pathways of ice-wedge degradation in polygonal tundra under different hydrological conditions, The Cryosphere Discussions, pp. 1–61, https://doi.org/10.5194/tc-2018-211, 2018.

Raynolds, M. K., Walker, D. A., Ambrosius, K. J., Brown, J., Everett, K. R., Kanevskiy, M., Kofinas, G. P., Romanovsky, V. E., Shur, Y., and Webber, P. J.: Cumulative geoecological effects of 62 years of infrastructure and climate change in ice-rich permafrost landscapes, Prudhoe Bay Oilfield, Alaska, Global Change Biology, 20, 1211–1224, https://doi.org/10.1111/gcb.12500, https://onlinelibrary.wiley.com/doi/abs/10.1111/gcb.12500, 2014.

Romanovsky, V., Sergueev, D., and Osterkamp, T.: Temporal variations in the active layer and near-surface permafrost temperatures at the long-term observatories in northern Alaska., 2003.

Romanovsky, V. E. and Osterkamp, T. E.: Thawing of the Active Layer on the Coastal Plain of the Alaskan Arctic, Permafrost and Periglacial Processes, 8, 1–22, https://doi.org/10.1002/(SICI)1099-1530(199701)8:1<1::AID-PPP243>3.0.CO;2-U, 1997.

Serreze, M. C. and Barry, R. G.: Processes and impacts of Arctic amplification: A research synthesis, Global and Planetary Change, 77, 85 – 96, https://doi.org/https://doi.org/10.1016/j.gloplacha.2011.03.004, http://www.sciencedirect.com/science/article/pii/S0921818111000397, 2011.

Stern, G. and Gaden, A.: From Science to policy in the Western and Central Canadian Arctic: An Integrated Regional Impact Study (IRIS) of Climate Change and Modernization, p. 432 pp., 2015.

Stieglitz, M., Déry, S. J., Romanovsky, V. E., and Osterkamp, T. E.: The role of snow cover in the warming of arctic permafrost, Geophysical Research Letters, 30, https://doi.org/10.1029/2003GL017337, 2003.

Stuefer, S., Homan, J., Kane, D., Gieck, R., and Youcha, E.: Snow Survey Results for the Central Alaskan Arctic, Arctic Circle to Arctic Ocean: Spring 2013, University of Alaska Fairbanks, Water and Environmental Research Center, Report INE/WERC, 2014.

Stuefer, S. L., Homan, J. W., Youcha, E. K., Kane, D. L., and Gieck, R. E.: Snow survey data for the central north slope watersheds: spring 2012, University of Alaska Fairbanks, Water and Environmental Research Center, Report INE/WERC, 12, 2012.

Walker, D., Raynolds, M., Buchhorn, M., and Peirce, J.: Landscape and permafrost change in the Prudhoe Bay Oilfield, Alaska, Alaska Geobotany Center, University of Alaska, AGC Publication, pp. 14–01, 2014.

Walker, D. A. and Everett, K. R.: Loess Ecosystems of Northern Alaska: Regional Gradient and Toposequence at Prudhoe Bay, Ecological Monographs, 61, 437–464, https://doi.org/10.2307/2937050, 1991.

Walker, D. A., Everett, K., Webber, P., and Brown, J.: Geobotanical atlas of the Prudhoe Bay region, Alaska, US Army Corps of Engineers, Cold Regions Research and Engineering Laboratory, Hanover, New Hampshire, U.S.A., 1980.

Walker, D. A., Buchhorn, M., Raynolds, M. K., Kanevskiy, M. Z., Matyshak, G. V., Shur, Y., and Peirce, J.: Effects of 45 Years of Heavy Road Traffic and Infrastructure on Permafrost and Tundra at Prudhoe Bay, Alaska, AGU Fall Meeting Abstracts, GC23J-1215, 2015.

Westermann, S., Langer, M., Boike, J., Heikenfeld, M., Peter, M., Etzelmüller, B., and Krinner, G.: Simulating the thermal regime and thaw processes of ice-rich permafrost ground with the land-surface model CryoGrid 3, Geoscientific Model Development Discussions, 9, 523 – 546, https://doi.org/10.5194/gmd-9-523-2016-supplement, https://hal-insu.archives-ouvertes.fr/insu-01387523, 2016.

Zhang, T.: Influence of the seasonal snow cover on the ground thermal regime: An overview, Reviews of Geophysics, 43, https://doi.org/10.1029/2004RG000157, 2005.

Zhang, T., Osterkamp, T. E., and Stamnes, K.: Some Characteristics of the Climate in Northern Alaska, U.S.A., Arctic and Alpine Research, 28, 509–518, https://doi.org/10.1080/00040851.1996.12003204, 1996.

Zhang, T., Barry, R. G., Knowles, K., Heginbottom, J. A., and Brown, J.: Statistics and characteristics of permafrost and ground-ice distribution in the Northern Hemisphere, Polar Geography, 23, 132–154, https://doi.org/10.1080/10889379909377670, https://doi.org/10.1080/10889379909377670, 1999.

ERKLÄRUNG

Ich erkläre, dass ich die vorliegende Arbeit nicht für andere Prüfungen eingereicht, selbständig und nur unter Verwendung der angegebenen Literatur und Hilfsmittel angefertigt habe. Sämtliche fremde Quellen inklusive Internetquellen, Grafiken, Tabellen und Bilder, die ich unverändert oder abgewandelt wiedergegeben habe, habe ich als solche kenntlich gemacht. Mir ist bekannt, dass Verstöße gegen diese Grundsätze als Täuschungsversuch bzw. Täuschung geahndet werden.

Berlin, den 06. Februar 2019

Oehme

Alexander Oehme